15. Kimura, K. D., Tissenbaum, H. A., Liu, Y. & Ruvkun, G. *daf-2*, an insulin receptor-like gene that regulates longevity and diapause in *Caenorhabditis elegans*. *Science* **277,** 942–946 (1997).
16. Paradis, S., Ailion, M., Toker, A., Thomas, J. H. & Ruvkun, G. A PDK1 homolog is necessary and sufficient to transduce AGE-1 PI3 kinase signals that regulate diapause in *Caenorhabditis elegans*. *Genes Dev.* **13,** 1438–1452 (1999).
17. Larsen, P. L., Albert, P. S. & Riddle, D. L. Genes that regulate both development and longevity in *Caenorhabditis elegans*. *Genetics* **139,** 1567–1583 (1995).
18. Dorman, J. B., Albinder, B., Shroyer, T. & Kenyon, C. The *age-1* and *daf-2* genes function in a common pathway to control the lifespan of *Caenorhabditis elegans*. *Genetics* **141,** 1399–1406 (1995).
19. Ogg, S. *et al.* The fork head transcription factor DAF-16 transduces insulin-like metabolic and longevity signals in *C. elegans*. *Nature* **389,** 994–999 (1997).
20. Lin, K., Dorman, J. B., Rodan, A. & Kenyon, C. *daf-16*: an HNF-3-forkhead family member that can function to double the life-span of *Caenorhabditis elegans*. *Science* **278,** 1319–1322 (1997).
21. Riddle, D., Swanson, M. & Albert, P. Interacting genes in nematode dauer larva formation. *Nature* **290,** 668–671 (1981).
22. Golden, J. & Riddle, D. The *Caenorhabditis elegans* dauer larva: developmental effects of pheromone, food, and temperature. *Dev. Biol.* **102,** 368–378 (1984).
23. Vowels, J. & Thomas, J. Genetic analysis of chemosensory control of dauer formation in *Caenorhabditis elegans*. *Genetics* **130,** 105–123 (1992).
24. Coburn, C. M., Mori, I., Ohshima, Y. & Bargmann, C. I. A cyclic nucleotide-gated channel inhibits sensory axon outgrowth in larval and adult *Caenorhabditis elegans*: a distinct pathway for maintenance of sensory axon structure. *Development* **125,** 249–258 (1998).
25. Ailion, M., Inoue, T., Weaver, C. I., Holdcraft, R. W. & Thomas, J. H. Neurosecretory control of aging in *Caenorhabditis elegans*. *Proc. Natl Acad. Sci. USA* **96,** 7394–7397 (1999).
26. Apfeld, J. & Kenyon, C. Cell nonautonomy of *C. elegans daf-2* function in the regulation of diapause and life span. *Cell* **95,** 199–210 (1998).
27. Lawless, J. F. *Models and Methods for Lifetime Data* (Wiley, New York, 1982).

Acknowledgements

We thank J. Whangbo, S. Alper, J. Alcedo, H. Hsin, K. Lin, L. Yang, Q. Ch'ng, A. Dillin, D. Garigan and other members of the Kenyon Lab, as well as members of Cori Bargmann's lab, for stimulating discussions. Some nematode strains were provided by the *Caenorhabditis* Genetics Center, which is funded by the NIH. J.A. was supported by an HHMI Predoctoral Fellowship. This work was supported by a grant from the NIA to C.K.

Correspondence and requests for materials should be addressed to C.K. (e-mail: ckenyon@biochem.ucsf.edu).

Atomic scale movement of the voltage-sensing region in a potassium channel measured via spectroscopy

Albert Cha*, Gregory E. Snyder†, Paul R. Selvin† & Francisco Bezanilla*

* *Department of Physiology and Department of Anesthesiology, UCLA School of Medicine, Los Angeles, California 90095, USA*
† *Department of Physics and Biophysics Center, University of Illinois at Urbana-Champaign, Urbana, Illinois 61801, USA*

Voltage-gated ion channels are transmembrane proteins that are essential for nerve impulses and regulate ion flow across cell membranes in response to changes in membrane potential. They are made up of four homologous domains or subunits, each of which contains six transmembrane segments[1,2]. Studies of potassium channels have shown that the second (S2) and fourth (S4) segments contain several charged residues, which sense changes in voltage and form part of the voltage sensor[3–5]. Although these regions clearly undergo conformational changes in response to voltage[6–10], little is known about the nature of these changes because voltage-dependent distance changes have not been measured. Here we use lanthanide-based resonance energy transfer[11,12] to measure distances between *Shaker* potassium channel subunits at specific residues. Voltage-dependent distance changes of up to 3.2 Å were measured at several sites near the S4 segment. These movements directly correlated with electrical measurements of the voltage sensor, establishing the link between physical changes and electrical charge movement. Measured distance changes suggest that the region associated with the S4 segment undergoes a rotation and possible tilt, rather than a large transmembrane movement, in response to voltage. These results demonstrate the first *in situ* measurement of atomic scale movement in a transmembrane protein.

Lanthanide-based resonance energy transfer (LRET) is a modification of conventional fluorescence resonance energy transfer in which a long-lived lanthanide donor transfers energy in a distance-dependent manner to a conventional organic fluorescent acceptor[11,12]. This technique has previously been used to measure Angstrom-scale conformational changes in proteins[13]. Here, specific sites in the channel were fluorescently labelled by substituting a cysteine for a particular residue and attaching cysteine-reactive compounds of either a donor, a terbium-chelate maleimide (TbM), or an acceptor, fluorescein maleimide (FM), to the same site in the four identical subunits of the channel (Fig. 1a; see also Methods).

Although this labelling leads to a heterogeneous population of channels with different numbers of donors and acceptors, associated problems are greatly minimized for three reasons. In LRET, only donor–acceptor pairs generate sensitized emission signals (that is, delayed emission of the acceptor after receiving energy from the donor), and channels that contain all donors or all acceptors do not contribute to the signal[11,12]. Also, with four-fold symmetry of the channel[14,15], there are only two possible intersubunit distances: the distance between residues on neighbouring subunits and the distance between residues across the pore, which are related by the Pythagorean theorem (Fig. 1a). Finally, the labelling is done so that there is typically only one acceptor per channel, which can readily accept energy independently from multiple donors.

Intersubunit distances were examined at specific sites near S2, in the S3–S4 linker and S4, and near the channel pore (Fig. 2, Table 1). The intersubunit distances (Fig. 1c and Methods) were calculated using the time constants of acceptor-sensitized emission and donor emission without an acceptor. Donor lifetime in the absence of an acceptor was independent of voltage at all sites, indicating no significant change in the environment of the caged terbium (data not shown). The sensitized emission displayed two time constants at all sites measured, reflecting two donor–acceptor distances that follow a Pythagorean relationship (Fig. 1c). This verifies that the technique is measuring distances between contiguous subunits and across the pore. The distance measured at F425C across the pore (30 Å) corresponds well to the distance obtained between α-carbons for the homologous residue from the crystal structure of the bacterial analogue, KcsA (29 Å) (ref. 14). This confirms that the technique is capable of obtaining realistic estimates of distance, as the KcsA pore has been shown to be similar to the *Shaker* pore in its ability to bind specific inhibitors of *Shaker*[16]. However, LRET, like other energy transfer techniques, is better at measuring relative distances or changes in distance than absolute distances. Potential sources of error, such as anisotropy of the fluorophores and uncertainty in the fluorophore's position with respect to the labelled residue due to the linker, have been addressed (see Methods).

Next, voltage-dependent movements near the voltage-sensing regions were measured by determining intersubunit distances as a function of voltage. Residue S346C demonstrated a robust voltage-dependent change in energy transfer as measured by sensitized emission lifetimes 50 ms after changing the voltage (Fig. 3a). This change is probably consistent with a voltage-dependent movement of ~3.2 Å between S346C residues on contiguous subunits as the channel moves into the open state (Fig. 3b). The voltage-dependent movement of S346C also coincides with the gating charge movement for the same channels, as determined by parameters of a sequential three-state model fit[21] to both values (Fig. 3c). The striking agreement between the measured distance changes and electrical charge movement strongly indicates that the observed movement of S346C residues is closely correlated with the movement of charged residues involved in channel gating.

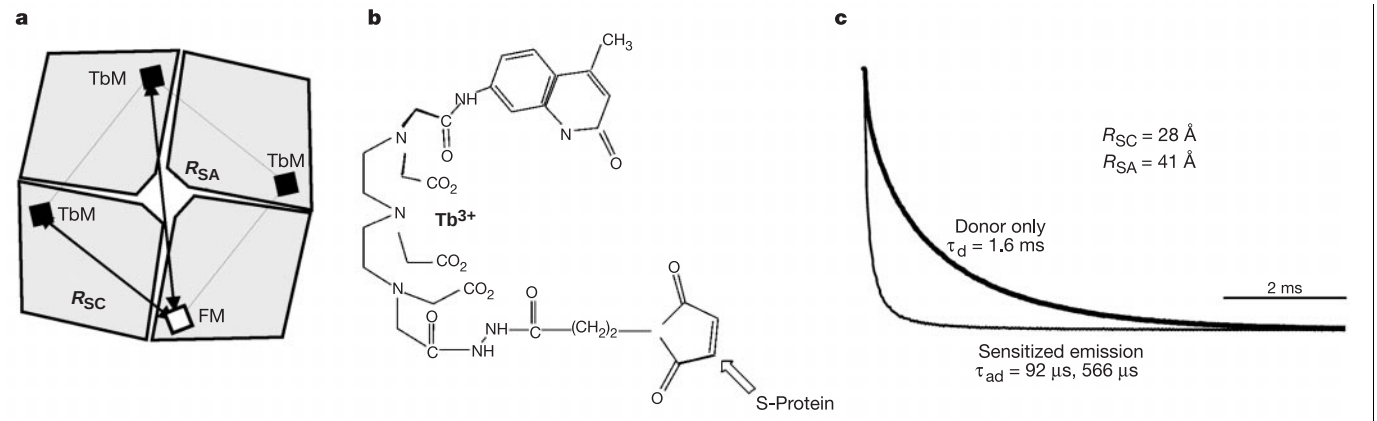

Figure 1 Labelling methodology and characteristics of ion channel. **a**, Labelling scheme of the channel's four identical subunits. About 70% of the channels that generate sensitized emission have three terbium-labelled subunits (TbM, closed squares) and one fluorescein-labelled subunit (FM, open square). With four-fold symmetry, the two measured distances between donor and acceptor are R_{SC} (between contiguous subunits) and R_{SA} (across the pore), related by the Pythagorean equation $R_{SA}^2 = 2R_{SC}^2$. **b**, Structure of the donor terbium-maleimide chelate, with dimensions of approximately 13 × 8 × 8 Å (ref. 24). S-protein represents the ion channel cysteine residue that attaches to the maleimide ring. **c**, Excited-state lifetimes used to deduce distances at site S346C. The terbium donor-only emission (thick trace) and fluorescein-sensitized emission (thin trace) are fitted to exponential decay functions, and the two corresponding time constants are used to compute two different distances (see Methods). Assuming that the shorter distance is R_{SC}, R_{SA} can be predicted from the measured R_{SC} (40 Å) and compared to the measured value (41 Å).

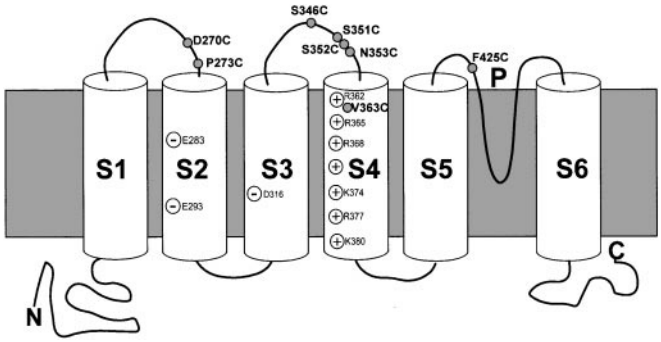

Figure 2 Transmembrane topology of the *Shaker* potassium channel. Cysteine-substituted sites examined with LRET measurements are denoted by grey circles and labelled in bold. Residues that constitute part of the voltage sensor are labelled and denoted as positively (+) and negatively (–) charged. P denotes the pore; C and N denote the C and N termini, respectively.

Table 1 Intersubunit distances and voltage-dependent changes measured using LRET

Location	Site	R_{SC} (Å)	R_{SA} (Å)	R_{SA} from R_{SC} (Å)	Standard error R_{SC}, R_{SA}	Anisotropy constraints (+%, –%)
S1–S2 loop	D270C	31	45	43	0.5, 0.6 $n = 9$	+6%, –3.8%
	P273C	32	47	46	0.7, 1.1 $n = 9$	+5.5%, –3.4%
S3–S4 loop	S346C	**26**–30	**37**–42	**37**–42	0.5, 0.7 $n = 5$	+4.5%, –2.7%
	S351C	28	**41**–42	40	0.4, 1.1 $n = 3$	+6.0%, –3.9%
	S352C	29	40	41	0.5, 1.6 $n = 13$	+5.3%, –3.3%
	N353C	29	42–**44**	41	0.6, 1.3 $n = 5$	+5.8%, –3.7%
S4	V363C	32	45	45	0.5, 0.6 $n = 7$	+5.4%, –3.3%
Pore	F425C		30	29	0.5 $n = 6$	

Shown are the measured distances between subunits (R_{SC}) and across the pore (R_{SA}) with standard error (n = number of oocytes) for sites throughout the channel. The estimated R_{SA} is calculated from the measured R_{SC}. The distance ranges given for S346C, S351C, and N353C indicate voltage-dependent distance changes from the closed (in bold) to the open state. The maximum error attributable to changes in the orientation factor κ^2 (last column) reflect the most extreme error possible, with a standard error of <0.2% (see Methods).

Energy transfer changes can arise not only from distance changes but also from a rotation of the acceptor or from spectral changes in the donor or acceptor. However, the magnitude of the energy transfer and distance changes at S346C is larger than could be attributed to a rotation of the acceptor, which could cause a worst-case apparent change of ~2 Å (+4.5% or –2.7% of the 26–29 Å distance between subunits at this site) (Table 1). The actual error is likely to be considerably less (see Methods). Similarly, a 50% change in the spectral overlap, which would be necessary to account for the energy transfer changes, is inconsistent with the voltage-dependent acceptor intensity change of <2% measured at this site.

It is conceivable that the donor or acceptor attached to S346C undergoes movement without an underlying protein conformational change owing to a change in the local potential gradient. However, the accessibility of site S346C to charged fluorophores is independent of voltage, and there is very little voltage-dependent change in fluorescence intensity, anisotropy, or emission spectra from fluorophores placed at the site (data not shown). Furthermore, if the electric field affected the position of the dyes, one would expect to see distance changes at site V363C which is expected to be in the strongest electric field of all the residues tested, because it lies between two of the gating charges in S4. However, V363C shows no intersubunit change in distance with voltage. Also, a voltage-dependent movement of the dyes, independent of the protein, would probably not correlate well with gating charge movement. Thus, it is likely that the measured distance changes are caused by protein conformational changes, and not caused by movement of the dye(s) alone.

It is surprising that movements (at S346C) can be detected at residues as many as 16 amino acids from the critical charged residues in S4, and that these movements show a voltage dependence of movement mirroring that of the electrical charge displacement. This result implies that the S3–S4 linker has a stiff secondary structure that allows movements of S4 to be faithfully transmitted throughout the linker. According to our measured distances in the S3–S4 linker in the closed state, sites further into the loop (such as S346C) are closer to each other (37 Å) than sites closer to S4 (V363C at 45 Å). This suggests that the S3–S4 loop may be tilted with respect to the channel's central axis in the closed state. In the open state, distances at these residues suggest that the S3–S4 linker is less tilted (Table 1). If S4 is aligned with the S3–S4 loop, S4 may also undergo a tilt in response to voltage. This hypothesis is also consistent with the larger movements seen at S346C than at sites closer to S4.

Voltage-dependent energy transfer changes were also detected at successive sites near S4, at S351C, S352C and N353C. Unexpectedly, the changes are different for each site (Fig. 4a). If the energy-transfer changes are caused by a physical translation, fluorophores at site S351C move ~1 Å further apart as the channel opens, site S352C shows no significant change in distance, and site N353C moves ~1 Å closer together. A simple model consistent with this data involves a rotation of this protein region. Fig. 4b portrays this region of the protein as an α-helix, which undergoes a rotation moving S351C further from the pore, N353C closer to the pore, and maintaining S352C at the same distance. It is also possible that the energy-transfer changes at these sites are caused by a reorientation of the acceptor without a corresponding translation. However, either interpretation supports a rotation of these three residues.

Movement in the plane of the membrane, which causes distance changes between subunits, can be measured with our technique. In addition, transmembrane movements can also be measured. At small depolarizations, some voltage sensors are in the activated position, while others are in the deactivated position, giving rise to distance changes between subunits with voltage (Fig. 5a, Active). In contrast, at very hyperpolarized (Fig. 5a, Closed) or depolarized (Fig. 5a, Open) potentials, the distance between subunits would be the same in either state. Assuming that the movements of the voltage sensors are independent with a transmembrane movement of 16 Å, as has been proposed[7,17], the intersubunit distance versus voltage would demonstrate a bell-shaped voltage dependence with a peak change in distance of 2.2 Å at intermediate potentials (Fig. 5b). As the actual voltage-dependent movement has a very different shape (Fig. 3b) and no such bell-shaped voltage-dependent movement was measured in or near S4, it is unlikely that this region undergoes a large non-cooperative transmembrane movement with voltage.

If the S3–S4 region is undergoing a rotation and possible tilt, what is the motion of S4, where the critical charged residues affected by the external electric field reside? S4 could undergo a large translation which, via a kink, leads to a rotation and tilting of S3–S4. However, the lack of distance changes at V363C, which is in S4, argues against this. Hence, we think it more likely that S4 itself is undergoing a rotation which drives the rotation seen in S3–S4.

These results are the first to measure actual voltage-induced distance changes in an ion channel. The movements at the particular residues measured correlate very well with electrical movement of charged residues in the voltage sensor. Our results imply that the voltage sensor need not undergo a large conformational change, as previously proposed[7,17]. One physical model that is consistent with our data and previous studies is shown in Fig. 5c. In the closed and open states of the channel, residues in and near the S4 segment reside in crevices within the protein for which histidine-associated protons have deeper accessibility than cysteine-reactive reagents[7,8]. The two crevices must be very close, separated by a non-conducting (hydrophobic) region, formed by the S4 itself. A small

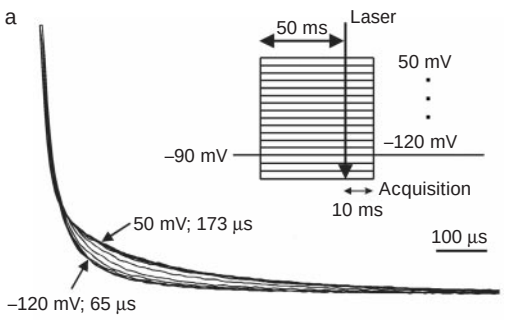

c

	Z_1	V_1	Z_2	V_2
R_{SC}	1.7	–67 mV	3.1	–54 mV
Q	1.3	–67 mV	2.3	–50 mV

Figure 3 Voltage-dependent distance changes at residue S346C and correlation to gating charge movement. **a**, Voltage-dependent sensitized emission changes measured at site S346C from 65 µs at –120 mV to 173 µs at 50 mV, measured 50 ms after a pulse to voltages –120 mV and 50 mV in increments of 10 mV. Inset, protocol. **b**, Movement of S346C between contiguous subunits (R_{SC}, open circles) and gating charge displacement (Q, black squares) as a function of voltage (error bars: standard error, $n = 5$). Both R_{SC} (thin line) and Q (thick line) were fitted to a sequential three-state model (see Methods). **c**, Parameters of the sequential two-Boltzmann fit for R_{SC} and Q, where Z_i and V_i represent the valence and voltage midpoint of the ith Boltzmann (see Methods).

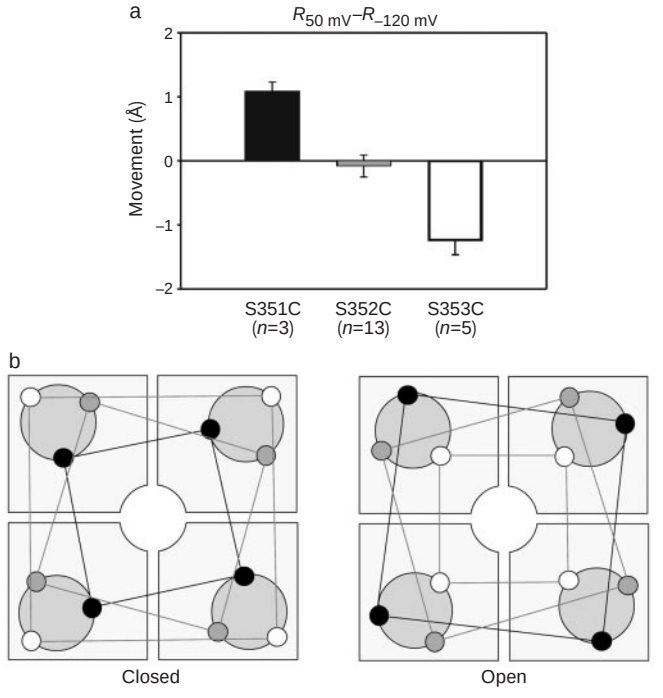

Figure 4 Distance changes at three successive residues in the S3–S4 linker. **a**, Distance changes in R_{SA} measured at successive residues; S351C (black, 1.1 Å further apart at 50 mV), S352C (grey, no change), and N353C (white, 1.3 Å closer together at 50 mV). Changes in distance from the open state ($R_{50\,mV}$) to the closed state ($R_{-120\,mV}$) were determined by measuring sensitized-emission lifetimes at different voltages in the same oocyte, and results from several oocytes were averaged with standard error (bars) shown. **b**, A physical model which leads to the distance modulation seen in **a**. If S351 (black), S352 (grey), and N353 (white) are members of an α-helix which rotates 180° as the channel opens, then S351 will move further apart, S352 will maintain the same distance, and N353 will move closer together. For clarity, the rotation is shown as 180°; however, the actual angle may be considerably less.

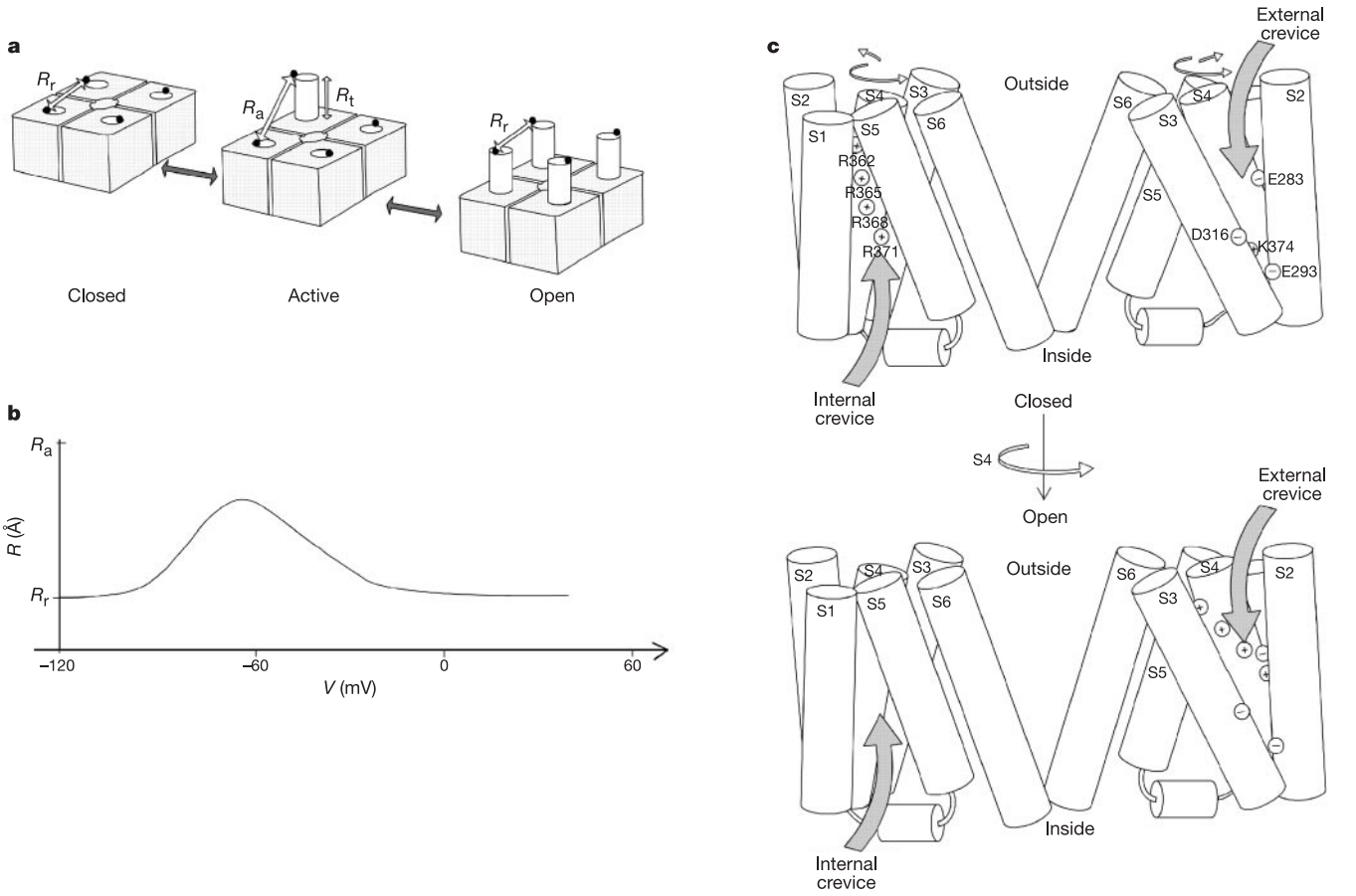

Figure 5 Translation versus rotation models of S4 movement. **a**, Diagram of a large S4 movement perpendicular to the membrane. Each subunit (square block) contains a moveable S4 (cylinder). For the closed or open states (labelled), the distance between contiguous subunits (R_r) will remain constant, but will change to R_a at intermediate potentials (Active), where only one or two S4s are activated. **b**, A large transmembrane movement, as described in **a**, will generate a peak distance change at intermediate potentials which depends on R_r, R_t (distance moved by the S4) and the independence of subunit movement. Assuming independence of voltage sensor movement, $R_r = 30$ Å, and $R_t = 16$ Å, the distance change peaks at ~2.2 Å at intermediate potentials. **c**, Two of the four subunits, illustrating movement of the S4 consistent with the experimental data[25]. In the closed state, charged residues R362, R365, R368, and R371 in S4 (denoted by ⊕) lie within a narrow internal (labelled) crevice formed by S1 and S5 that opens into the intracellular solution. After the S4 undergoes a rotation (shown as 180°) and tilt, the charged residues become accessible to the extracellular solution via a narrow external crevice (labelled) formed by S2 and S3.

conformational change such as a rotation can then move the charge across the field, while changing chemical accessibility from the intracellular to the extracellular solution.

The present measurements give new insight into the physical rearrangements underlying gating in ion channels. The technique of LRET, particularly when combined with electrical measurements, can be used to study atomic scale structural changes in this channel and, in the future, other transmembrane proteins *in situ*. □

Methods

Distance computation

Energy transfer (E) is calculated by comparing the donor-only lifetime (τ_D) with the lifetime of the sensitized emission (τ_{AD}) using the relation $E = 1 - \tau_{AD}/\tau_D$. The distance (R) is then computed using the conventional formula, $R = R_0(E^{-1} - 1)^{1/6}$ where R_0 is a characteristic distance depending on choice of donor and acceptor: here $R_0 = 45$ Å (refs 18, 19). Multiple τ_{AD} lifetimes indicate that there are several different donor–acceptor pairs undergoing different amounts of energy transfer from which separate distances can be calculated. For distance changes, the acceptor-sensitized emission was fitted to distances constrained by the Pythagorean theorem.

Stoichiometry of labelling

Given the labelling ratio of 4:1 of terbium maleimide to fluorescein maleimide and a binomial distribution of subunit labelling, 41% of channels will have four donors, 41% will have three donors and one acceptor, 15% will have two donors and two acceptors, 2.6% will have three acceptors and one donor, and 1.6% will have four acceptors. The channels with four donors or four acceptors will not contribute to acceptor-sensitized emission, as there are no donor–acceptor pairs in these channels. The small subpopulation of channels with two donors and two acceptors will yield different distances, as each donor sees two nearby acceptors instead of one. However, the error is very small for this 15% subpopulation of channels: ~1.4 Å for a distance of 28 Å. This error is also nearly eliminated when measuring differences in distances, such as changes in distance as a function of voltage.

Sources of error in distance measurements

R_0 is affected by the anisotropy of donor and acceptor. The donor is inherently unpolarized (G. E. Snyder & P. R. Selvin, unpublished data). The anisotropy of fluorescein, which is a measure of its nanosecond-scale wobble, was determined at different channel sites, and maximum error estimates resulting from these anisotropy values have been included in the table for each site (see Supplementary Information). Additional wobble during the micro- to millisecond donor lifetime further reduces this error. The other source of uncertainty is the variability of the fluorophore's position with respect to the labelled residue, owing to the length of the maleimide linker. If the probes either sweep out a large volume, or are far from their attachment sites with the donor sitting at a significantly different position from the acceptor, then the four-fold symmetry breaks down. Consequently, the Pythagorean relationship between distances across (R_{SA}) and contiguous (R_{SC}) to the pore would no longer be valid. In fact, the deviation from the Pythagorean relationship depends on the size of the volume sampled and the flexibility of the linker. For instance, if the linkers permit the fluorophores to sample a volume with a 10 Å radius, and they are attached to residues located 50 Å apart, then the measured contiguous distance would be ~30 Å because the R^{-6} power dependence places the heaviest weight on the closest distance between fluorophores. In that case, the difference between the predicted distance (from Pythagorean theorem) and the measured distance is 7 Å. However, our measured and predicted distances from the Pythagorean theorem are typically within 1–2 Å. The error introduced by flexibility of the linker is therefore <2 Å and would not account for our measured distance changes.

Experimental protocols

The fast inactivation-removed, non-conducting version of the *Shaker* K^+ channel (H4IR) was used, and site-directed mutagenesis, transcription of cRNA, and experimental solutions were carried out as described[20]. Oocytes were rinsed in a sterile SOS without DTT and labelled with 2 μM TbM and 0.5 μM FM for 30 min at 18 °C. Gating, ionic, and fluorescence currents were acquired as described[20]. The optical setup consisted of a Zeiss Axiovert 10 with a 337-nm nitrogen laser (Laser Science; Newton, MA) as light source, and a 350-nm dichroic with a long pass filter 515 nm in length for donor-only fluorescence or a 510–530 nm filter for sensitized emission (Omega Optical). A custom oocyte chamber was designed to view the clamped oocyte surface in an inverted cut-open configuration using a fused quartz 20× objective with numerical aperture 0.65 (Partec). A voltage electrode was inserted from above into the oocyte interior to measure the transmembrane potential for the virtual ground voltage clamp. Light measurements were made with a gallium arsenide R943-02 photomultiplier tube (PMT) (Hamamatsu), with gate normally on option, operated at 800–1,400 V with an S502 power supply and cooled to −25 °C with a TE104RF PMT cooler (Products for Research). A TTL pulse was used to turn off the PMT during the laser pulse to avoid saturation. The current output of the assembly was amplified with a current-to-voltage converter with a 1-MΩ feedback resistor and was filtered at 20 kHz.

Three-state model

The equation used to fit the distance (R_{sc}) and gating charge displacement (Q) was

$$f(V) = a + \frac{bz_0[1+\exp(-z_1e(V-V_1)/kT)]}{1+\exp(-z_1e(V-V_1)/kT)[1+\exp(-z_0e(V-V_0)/kT)} + \frac{bz_1}{1+\exp(-z_1e(V-V_1)/kT)[1+\exp(-z_1e(V-V_0)/kT)]}$$

where z_0 and z_1 are the valences and V_0 and V_1 are the midpoints of the two sequential steps. For R_{SC}, a is the minimum distance and $b(z_0+z_1)$ is the maximum distance change. For Q, $a=0$ and $b(z_0+z_1)=1$. This equation reflects the minimum model that is appropriate to fit the charge movement of the voltage sensor[21].

Model assumptions

It is conceivable, but unlikely, that the voltage sensors in each channel are so highly cooperative that all voltage sensors move simultaneously at all potentials, preventing the intermediate state in Fig. 4b from occurring. Cooperativity in *Shaker* has been shown, but occurs in transitions close to the open state at voltages where most of the gating charge has already moved[22,23]. Also, most kinetic models of the *Shaker* potassium channel utilize four subunits which behave independently at hyperpolarized potentials, and then undergo a cooperative, concerted transition into the open state[23]. Evidence in sodium channels also indicates that at intermediate potentials, some subunits' voltage sensors are activated, while other subunits' voltage sensors are deactivated (see Supplementary Information).

Received 22 July; accepted 19 October 1999.

1. Noda, M. *et al*. Primary structure of the *Electrophorus electricus* sodium channel deduced from cDNA sequence. *Nature* **312,** 121–127 (1984).
2. Tempel, B. L., Papazian, D. M., Schwarz, T. L., Jan, Y. L. & Jan, L. Y. Sequence of a probable potassium channel component encoded at *Shaker* locus of *Drosophila*. *Science* **237,** 770–775 (1987).
3. Armstrong, C. M. & Bezanilla, F. Currents related to the movement of the gating particles of sodium channels. *Nature* **242,** 459–461 (1973).
4. Seoh, S. A., Sigg, D., Papazian, D. M. & Bezanilla, F. Voltage-sensing residues in the S2 and S4 segments of the Shaker K+ channel. *Neuron* **16,** 1159–1167 (1996).
5. Aggarwal, S. K. & MacKinnon, R. Contribution of the S4 segment to gating charge in the Shaker K+ channel. *Neuron* **16,** 1169–1177 (1996).
6. Yang, N. & Horn, R. Evidence for voltage-dependent S4 movement in sodium channels. *Neuron* **15,** 213–218 (1995).
7. Larsson, H. P., Baker, O. S., Dhillon, D. S. & Isacoff, E. Y. Transmembrane movement of the Shaker K+ channel S4. *Neuron* **16,** 387–397 (1996).
8. Starace, D. M., Stefani, E. & Bezanilla, F. Voltage-dependent proton transport by the voltage sensor of the Shaker K+ channel. *Neuron* **19,** 1319–1327 (1997).
9. Mannuzzu, L. M., Moronne, M. M. & Isacoff, E. Y. Direct physical measure of conformational rearrangement underlying potassium channel gating. *Science* **271,** 213–216 (1996).
10. Cha, A. & Bezanilla, F. Characterizing voltage-dependent conformational changes in the Shaker K+ channel with fluorescence. *Neuron* **19,** 1127–1140 (1997).
11. Selvin, P. R. & Hearst, J. E. Luminescence energy transfer using a terbium chelate: improvements on fluorescence energy transfer. *Proc. Natl Acad. Sci. USA* **91,** 10024–10028 (1994).
12. Selvin, P. R., Rana, T. M. & Hearst, J. E. Luminescence resonance energy transfer. *J. Am. Chem. Soc.* **116,** 6029–6030 (1994).
13. Xiao, M. *et al*. Conformational changes between the active-site and regulatory light chain of myosin as determined by luminescence resonance energy transfer: the effect of nucleotides and actin. *Proc. Natl Acad. Sci.* **95,** 15309–15314 (1998).
14. Doyle, D. A. *et al*. The structure of the potassium channel: molecular basis of K+ conduction and selectivity. *Science* **280,** 69–77 (1998).
15. Gross, A., Columbus, L., Hideg, K., Altenbach, C. & Hubbell, W. L. Structure of the KcsA potassium channel from *Streptomyces lividans*: A site-directed spin labeling study of the second transmembrane segment. *Biochemistry* **38,** 10324–10335 (1999).
16. MacKinnon, R., Cohen, S.L., Kuo, A., Lee, A. & Chait, B. T. Structural conservation in prokaryotic and eukaryotic potassium channels. *Science* **280,** 106–109 (1998).
17. Durell, S. R. & Guy, H. R. Atomic scale structure and functional models of voltage-gated potassium channels. *Biophys. J.* **62,** 238–247 (1992).
18. Selvin, P. R. Fluorescence resonance energy transfer. *Methods Enzymol.* **246,** 300–344 (1995).
19. Chen, J. & Selvin, P. R. Thiol-reactive luminescent chelates of terbium and europium. *Bioconjugate Chem.* **10,** 311–315 (1999).
20. Cha, A. & Bezanilla, F. Structural implications of fluorescence quenching in the Shaker K+ channel. *J. Gen. Phys.* **112,** 391–408 (1998).
21. Bezanilla, F., Perozo, E. & Stefani, E. Gating of Shaker K+ channels: II. The components of gating currents and a model of channel activation. *Biophys. J.* **66,** 1011–1021 (1994).
22. Smith-Maxwell, C. J., Ledwell, J. L. & Aldrich, R. W. Uncharged S4 residues and cooperativity in voltage-dependent potassium channel activation. *J. Gen. Phys.* **111,** 421–439 (1998).
23. Schoppa, N. E. & Sigworth, F. Activation of Shaker potassium channels. III. An activation gating model for wild-type and V2 mutant channels. *J. Gen. Phys.* **111,** 313–342 (1998).
24. Selvin, P. R., Jancarik, J., Li, M. & Hung, L. W. Crystal structure and spectroscopic characterization of a luminescent europium chelate. *Inorg. Chem.* **35,** 700–705 (1996).
25. Bezanilla, F. The voltage sensor in voltage dependent ion channels. *Physiol. Rev.* (in the press).

Supplementary information is available on *Nature*'s World-Wide Web site (http://www.nature.com) or as paper copy from the London editorial office of *Nature*.

Acknowledgements

This work was supported by NIH grants to F.B. and P.R.S., the Hagiwara Chair funds to F.B., and from Research Corporation to P.R.S. A.C. was also supported by UCLA Medical Scientist Training Program and a National Research Service Award from National Institute of Mental Health. G.E.S. was supported by a National Research Service Award in Molecular Biophysics. We thank A. Gross, for his involvement in preliminary FRET results, and J. Chen, for synthesis of maleimide terbium chelates. We also thank the members of the Bezanilla lab for their support.

Correspondence and requests for materials should be addressed to F.B. (e-mail: fbezanil@ucla.edu) and P.R.S. (e-mail: selvin@uiuc.edu).

Spectroscopic mapping of voltage sensor movement in the *Shaker* potassium channel

K. S. Glauner, L. M. Mannuzzu, C. S. Gandhi & E. Y. Isacoff

Department of Molecular & Cell Biology, University of California, Berkeley, 271 Life Science Addition, Berkeley, California 94720-3200, USA

Voltage-gated ion channels underlie the generation of action potentials and trigger neurosecretion and muscle contraction. These channels consist of an inner pore-forming domain, which contains the ion permeation pathway and elements of its gates, together with four voltage-sensing domains, which regulate the gates[1–6]. To understand the mechanism of voltage sensing it is necessary to define the structure and motion of the S4 segment, the portion of each voltage-sensing domain that moves charged residues across the membrane in response to voltage change[7–14]. We have addressed this problem by using fluorescence resonance energy transfer as a spectroscopic ruler[15–17] to determine distances between S4s in the *Shaker* K^+ channel in different gating states. Here we provide evidence consistent with S4 being a tilted helix that twists during activation. We propose that helical twist contributes to the movement of charged side chains across the membrane electric field and that it is involved in coupling voltage sensing to gating.

Opening of voltage-gated channels is triggered by the depolarization-driven outward movement of the S4 segment through a transmembrane canal[1,7–14]. This motion generates a small gating current that reflects the movement of charged residues across the membrane electric field. Different types of transmembrane movement have been proposed, leading to distinct models describing how the membrane electric field drops across S4, the forces that S4 needs to overcome to move through the canal and the mechanism of coupling between S4 and the pore domain's gates.

In an attempt to understand how S4 moves we used fluorescence resonance energy transfer (FRET) to measure intersubunit distances between positions within and just outside S4 in both resting and